

Enhancing phase separation of double-chiral particles by regulating inter-chiral frustration

Yi-Chen Lu(陆羿辰), Wan-Rou Cai(蔡婉柔), Meng-Chu Wang(王梦楚), Ya-Li Liu(刘雅莉), Tong Zhu(朱童), Yi-Lin Zhou(周怡琳), Tian-Chen Yu(余天晨), Yun-Xuan Ji(纪蕴轩), Ming-Qian Ao(敖明茜), Chen-Lu Li(李晨璐), Cheng-Xu Yan(颜乘旭), and Zhi-Gang Zheng(郑志刚)

Citation: Chin. Phys. B, 2025, 34 (**8**): 080506. DOI: 10.1088/1674-1056/ade06f
http://cpb.iphy.ac.cn; http://iopscience.iop.org/cpb

What follows is a list of articles you may be interested in

Chaos of cavity optomechanical system with Coulomb coupling

Yingjia Yang(杨应佳), Liwei Liu(刘利伟), Lianchun Yu(俞连春), Weizheng Kong(孔伟正), Haiyan Jiao(焦海燕), Xiaoyan Deng(邓小燕), and Xiaoyong Li(李小勇)

Chin. Phys. B, 2025, 34 (**8**): 080503. DOI: 10.1088/1674-1056/add509

Generation of multitype, multicavity chaotic attractors via impulse-function-based state variable extension

Xiaoyu Hu(胡晓宇), Siteng Wang(王思腾), Panpan Wu(邬盼盼), Hongbo Cao(曹红博), Tianwei Yang(杨天纬), and Zhongshuo Dong(董忠硕)

Chin. Phys. B, 2025, 34 (**8**): 080502. DOI: 10.1088/1674-1056/add249

An enhanced fingerprint template protection scheme based on four-dimensional superchaotic system and dynamic DNA coding

Baiqiang Hu(胡百强), Jiahui Liu(刘嘉辉), and Zhe Liu(刘喆)

Chin. Phys. B, 2025, 34 (**7**): 070505. DOI: 10.1088/1674-1056/adca9f

Effects of noise on synchronization in simplicial complexes

Linying Xiang(项林英), Shuwei Yao(姚姝玮), Yining Chen(陈艺宁), Ruitong Yan(闫锐桐), and Ruya Xia(夏儒雅)

Chin. Phys. B, 2025, 34 (**7**): 070503. DOI: 10.1088/1674-1056/adc7ef

Analysis of the induction of the myelin basic protein binding to the plasma membrane phospholipid monolayer

Lei Zhang(张蕾), Changchun Hao(郝长春), Ying Feng(冯盈), Feng Gao(高峰), Xiaolong Lu(逯晓龙), Junhua Li(李俊花), Runguang Sun(孙润广)

Chin. Phys. B, 2016, 25 (**9**): 090507. DOI: 10.1088/1674-1056/25/9/090507

SPECIAL TOPIC — A celebration of the 90th Anniversary of the Birth of Bolin Hao

Enhancing phase separation of double-chiral particles by regulating inter-chiral frustration

Yi-Chen Lu(陆羿辰)[1,2,†], Wan-Rou Cai(蔡婉柔)[1,3,†], Meng-Chu Wang(王梦楚)[1,3], Ya-Li Liu(刘雅莉)[1,3], Tong Zhu(朱童)[1,3], Yi-Lin Zhou(周怡琳)[1,3], Tian-Chen Yu(余天晨)[1,3], Yun-Xuan Ji(纪蕴轩)[1,3], Ming-Qian Ao(敖明茜)[1,3], Chen-Lu Li(李晨璐)[1,3], Cheng-Xu Yan(颜乘旭)[1,3], and Zhi-Gang Zheng(郑志刚)[1,3,‡]

[1] *Institute of Systems Science, Huaqiao University, Xiamen* 361021, *China*
[2] *School of Mathematical Sciences, Huaqiao University, Quanzhou* 362021, *China*
[3] *College of Information Science and Technology, Huaqiao University, Xiamen* 361021, *China*

(Received 11 April 2025; revised manuscript received 10 May 2025; accepted manuscript online 4 June 2025)

Chiral active matter exhibits a variety of collective behaviors, including phase separation, which is governed by the rule of "like chiralities attract, while opposite chiralities repel". In this work, we investigate the chiral demixing strategy of double-chiral partial mixture with inter-chiral frustration. We find that the inter-chiral frustration can significantly enhance the chiral demixing of active particles with different chiralities, both during the transient and in the steady state, not only accelerating the progress, but also improving the degree of phase separation. This phenomenon is reminiscent of the phase separation of binary mixtures in condensed matter physics, where the inter-chiral frustration can play a crucial role in the formation of the phase-separated states. We construct the phase diagram of the system and discuss the critical frustration for the enhancement of chiral demixing. Our work presents the first systematic investigation of inter-chiral frustration in self-propelled chiral active matter, filling a critical gap in the field.

Keywords: chiral active matter, demixing, phase separation, frustration

PACS: 05.45.–a, 89.75.Kd, 11.30.Rd

DOI: 10.1088/1674-1056/ade06f **CSTR:** 32038.14.CPB.ade06f

1. Introduction

We live in a colorful world filled with systems composed of diverse individuals, spanning microscopic entities like bacteria[1,2] and colloidal Janus particles[3–6] to macroscopic agents such as humans,[7–9] animals[10–13] and robots.[14–16] These systems exhibit a wide range of collective phenomena, including cell migration,[17,18] clustering,[19–22] crystallization,[23,24] lane formations,[25–27] swirling formations,[28–31] low-Reynolds-number turbulence,[32–34] and even the emergence of negative viscosities.[35] For instance, biological groups display behaviors like the swarming dynamics of bird flocks[12,13,36,37] and the synchronized swimming of fish shoals.[10,11] Remarkably, such collective patterns extend beyond the scale of systems: superfluidity in bacterial teamwork[1,2] and collective oscillations in pedestrian crowds[7–9] reveal universal principles across scales. These behaviors not only inspire fascination but also hold profound implications for group survival and material science.

Chirality, a fundamental property inherent in many natural systems, significantly influences a variety of biological,[38,39] chemical,[40] and physical processes.[41,42] The chirality observed in molecules, cells, and organisms can give rise to a broad spectrum of phenomena, including the formation of helical structures[43] and the manifestation of chiral motion or trajectories. The scientific framework for understanding such motion was initially proposed by Bronn[44] and Jennings.[45] In recent years, the study of chiral active matter has garnered increasing attention due to its promising applications, such as enhancing our understanding of the collective behavior within biological systems[46,47] and facilitating the design of chiral materials.[48–51] Based on this, a series of theoretical works have been proposed to investigate the collective behaviors of chiral active matter,[37,52–56] which provide valuable insights into the mechanisms underlying the emergence of swarming phenomena. Beyond theoretical approaches, experimental studies have also been conducted to explore the dynamics of chiral active matter, including the investigation of emergent chirality in robots[14,15] and the observation of chiral active matter in self-propelled colloidal systems.[48,50]

In prior research, we investigated chirality-induced phase separation in chiral active matter, which obeys the principle of "like chiralities attract, while opposite chiralities repel".[57] This behavior aligns with observations in diverse chiral active matter systems.[53,54,58–60] Our analysis revealed that phase separation emerges robustly when chirally distinct populations exhibit a significant disparity in their natural frequencies. Con-

[†]These authors contributed equally to this work.
[‡]Corresponding author. E-mail: zgzheng@hqu.edu.cn
© 2025 Chinese Physical Society and IOP Publishing Ltd. All rights, including for text and data mining, AI training, and similar technologies, are reserved.

versely, when the frequency difference falls below a critical threshold, the two groups transition to a mixed state, marked by spatially overlapping configurations and synchronized dynamics. In the present study, we extend the model to include inter-chiral frustration. Inter-chiral frustration can be understood as an intrinsic form of geometric frustration arising from the interplay of chiral motion interactions. For instance, studies such as Refs. [61,62] explored this phenomenon using 3D-printed robots on vibrating tables, where competing rotational torques led to phase separation. Analogous behavior has been widely observed in soft and active matter systems.[63–66] For example, inter-chiral frustration emerges when bacteria interact with a substrate that imparts linear momentum,[2] where the phase dynamics of rotors coupled to fluid flow can be approximated by a Kuramoto-like model incorporating phase frustration determined by the torque (chirality). Our work presents the first systematic investigation of inter-chiral frustration in self-propelled particle systems, addressing a key gap in the field.

Strikingly, the inter-chiral frustration can significantly enhance the chiral demixing of the system, both during the transient and in the steady state, not only accelerating the progress, but also improving the degree of phase separation. For small frequency differences, the phase separation is more pronounced when the phase frustration is increased, which compensates for the lack of demixing degree at lower frequencies. This phenomenon is reminiscent of the phase separation of binary mixtures in condensed matter physics.[67–70]

The paper is organized as follows. In Section 2, we introduce the model and the order parameters used to quantify the chiral demixing of the system. In Section 3, we present the results of the numerical simulations and analyze the behaviors of the system under different conditions. In Section 4, we construct the phase diagram of the system and discuss the critical frustration for the complete demixing of the system. Finally, we conclude the paper in Section 5.

2. The model

Particles have a spatial position $\boldsymbol{r}_i = (x_i, y_i)$ and an internal phase θ_i which evolve according to equations

$$\dot{\boldsymbol{r}}_i = v\boldsymbol{p}(\theta_i), \tag{1a}$$

$$\dot{\theta}_i = \omega_i + \frac{K}{|A_i|}\sum_{j\in A_i}\left[\sin(\theta_j - \theta_i + \alpha_{ij}) - \sin\alpha_{ij}\right], \tag{1b}$$

for $i = 1, 2, \ldots, N$. Here in Eq. (1a), $\boldsymbol{p}(\theta) = (\cos\theta, \sin\theta)$, which means each particle rotates with a constant speed v in the direction of its instantaneous phase $\theta_i(t)$. The particles are treated as point-like with no direct spatial interactions, consistent with classical models of chiral self-propelled particles.[37,53–56] As per Eq. (1b), the mean runs over neighbors within a coupling radius d_0 around particle i

$$A_i(t) = \left\{ j \mid \left|\boldsymbol{r}_i(t) - \boldsymbol{r}_j(t)\right| \leqslant d_0 \right\}. \tag{2}$$

The K is the coupling strength, and ω_i is the natural frequency of the i-th particle. This means that a particle will rotate with the angular velocity $|\omega_i|$ in the absence of mutual coupling ($K = 0$), and the sign of ω_i represents the direction of rotation, namely, the attribute of the chirality of the i-th particle. A positive (negative) chirality (ω) describes the counterclockwise (clockwise) rotations of the particle in space. We will study particles including two types of chiralities with both positive and negative natural frequencies uniformly distributed in two symmetric regimes as

$$g_{\mathrm{U}}^{\mathrm{D}}(\omega;\mu,\sigma) = \frac{1}{2}\left[g_{\mathrm{U}}(\omega;-\mu,\sigma) + g_{\mathrm{U}}(\omega;\mu,\sigma)\right], \tag{3}$$

where $g_{\mathrm{U}}(\omega;\mu,\sigma)$ is the uniform distribution

$$g_{\mathrm{U}}(\omega;\mu,\sigma) = \begin{cases} \frac{1}{\sigma}, & \omega_{\min} \leqslant \omega \leqslant \omega_{\max}, \\ 0, & \text{otherwise}. \end{cases} \tag{4}$$

Here $\sigma = \omega_{\max} - \omega_{\min}$ is the natural-frequency span, and $\mu = (\omega_{\max} + \omega_{\min})/2$ is the average.

Additionally, α_{ij} is the phase frustration between two neighboring particles, which is defined as

$$\alpha_{ij} = \begin{cases} \alpha_0, & \omega_i\omega_j < 0, \\ 0, & \omega_i\omega_j \geqslant 0. \end{cases} \tag{5}$$

When $\alpha_0 = 0$, the dynamics reduces to the normal chiral model.[57] The counter term $\sin\alpha_{ij}$ is introduced to ensure that frustration only interferes with the inter-chiral coupling without changing the sign of effective frequency.

To isolate the deterministic effects of frequency mismatch and inter-chiral frustration, we omitted translational and rotational noise terms. Previous work[57] showed that strong translational noise mainly drives particle diffusion, whereas strong rotational noise disrupts phase synchronization. However, the potential nonlinear influence of moderate noise on system dynamics remains an open question — a topic we will investigate in future studies.

Some order parameters can be introduced to measure the level of spatiotemporal coordination among particles and distinguish the different collective states of the system. Firstly, an order parameter to measure the chiral demixing among particles can be defined as

$$S(t) = \frac{1}{N}\sum_{i=1}^{N}\frac{\sum_{j\in A_i} H(\omega_i\omega_j)}{|A_i(t)|}, \tag{6}$$

where $H(x) = (x > 0)$ is the Heaviside step function. $S(t)$ is the fraction of the pairs of neighboring particles with the same chirality. When $S(t) = 1$, all neighboring pairs share chirality, and the system is in a completely phase-separated state. When $S(t) < 1$, the system is in a mixed state.

Except for measuring the demixing degree, an order parameter to measure the degree of the complete demixing can be defined as

$$M(t)=\frac{1}{N}\sum_{i=1}^{N}H\left[\sum\nolimits_{j\in A_i}H\left(-\omega_i\omega_j\right)\right]. \tag{7}$$

The $M(t)$ is the fraction of particles that have neighbors with different chirality. When $M(t)=0$, the system is completely phase-separated. When $M(t)>0$, the system is in a mixed state. Obviously, M describes the qualitative nature of the complete demixing of the system, while S describes the partial demixing, which is a looser measure.

The above order parameters measure the chiral demixing from the perspective of the spatial distribution. The coordination of the internal phases can also be quantified to describe the demixing of the system. Firstly, a usual order parameter to measure the phase synchronization of the system can be defined as

$$Z(t)=R(t)\,\mathrm{e}^{\mathrm{i}\psi(t)}=\frac{1}{N}\sum_{j=1}^{N}\mathrm{e}^{\mathrm{i}\theta_j(t)}, \tag{8}$$

where $\mathrm{i}=\sqrt{-1}$. The degree modulus $R(t)=|Z(t)|$ is the absolute value of the mean of the complex numbers $\mathrm{e}^{\mathrm{i}\theta_i}$, which can be interpreted as the absolute value of the mean normalized velocity of all particles. When $R\approx 1$, particles are fully phase synchronized, and when $R\approx 0$, particles are phase incoherent. In a mixed state, the particles are phase locked with each other, and the order parameter R remains constant in the long run, while in the phase-separated state, the particles of different chiralities are uncoupled, then R will fluctuate over time. These behaviors can be quantified by the maximum and minimum values of R in a certain time window

$$R_{\max}=\max_{t\in W}\{R(t)\}, \tag{9a}$$

$$R_{\min}=\min_{t\in W}\{R(t)\}, \tag{9b}$$

where $W=[T-h,T+h]$ is a time window that is long enough to cover the transient and steady states of the system. When $R_{\max}=R_{\min}\approx 1$, the system is in a mixed state, and when $R_{\max}\neq R_{\min}$, the system is phase-separated.

We conducted numerical simulations to investigate the performance and characteristics of our system under various conditions. For simplicity, we assume that particles are initially distributed uniformly in a two-dimensional $L\times L$ square with periodic boundary conditions. To reduce the parameter space, we adopt dimensionless units by scaling space with d_0 and time with d_0/v. The system is then characterized by the following dimensionless parameters: the particle density $\rho_0=Nd_0^2/L^2$, the coupling strength $K'=Kd_0/v$, the natural frequency $\omega_i'=\omega_i d_0/v$, the phase frustration $\alpha_0'=\alpha_0$, and the coupling radius $d_0'=d_0/d_0=1$. Therefore, the particle density ρ_0 can be independently controlled by adjusting either the population size N or the box size L. Note that in Eq. (1b), the coupling term takes a mean-field-like form, which is also considered in the works of Ventejou *et al.*[54] and Wang *et al.*[55] For global all-to-all coupling, Eq. (1b) reduces to a chirality-frustrated Kuramoto model. Notably, when ρ_0 is sufficiently large, the system becomes insensitive to further increases in particle density, as discussed later at the end of Section 4. Remarkably, the phase diagram is primarily determined by the frustration α_0' and the rescaled natural frequency ω_i'. Since these depend directly on the original parameters α_0 and ω_i (with $\alpha_0'=\alpha_0$ and $\omega_i'\propto\omega_i$), we retain the original parameters in the main text for clarity and consistency with experimental controls. Unless otherwise stated, all the numerical simulations of the model Eq. (1) were run in Python using Euler integration with box size of $L=7$, population sizes of $N=1000$, coupling strength of $K=20$, self-propulsion speed of $v=3$, natural-frequency span $\sigma=1$, minimal absolute value of frequencies $\omega_{\min}$ in $\left[10^{-3},3\right]$, and coupling radius of $d_0=1$. For the final state and phase diagram, each data point of order parameters was collected by averaging the last 1000 time steps of the simulation to discard the transients.

3. Frustration-enhanced demixing

Inter-chiral frustration can significantly enhance the chiral demixing of the system, both during the transient and in the steady state. The spatial distribution of the particles is shown in Fig. 1 by modulating the minimal frequencies $\omega_{\min}$ and phase frustrations α_0. A mixed state is observed when the minimal frequency $\omega_{\min}\ll 1$ and phase frustration $|\alpha_0|\ll 1$ (see the snapshots (b)–(d) and (h) of Fig. 1), as the phase frustration is not strong enough to interfere with the inter-chiral coupling. When the minimal frequency $\omega_{\min}$ is increased, the difference in natural frequencies between two chiral substances becomes significant, and the system will phase separate into two clusters with the same chirality, which can be regarded as the self-organized phase separation of the system. As an external interference, the phase separation is more pronounced when the phase frustration α_0 is increased, as shown in Figs. 1(a), 1(e), 1(f), 1(j), 1(k), 1(o), and this effect can also be observed for minuscule frequency differences, which is illustrated in the first row of Fig. 1. Additionally, the sign of the frustration, $\mathrm{sgn}\alpha_0$, can also affect the spatial scale of the clusters. When the phase frustration α_0 is positive, clusters with positive chirality are more compact, whereas clusters with negative chirality tend to be more dispersed, as illustrated in Figs. 1(e), 1(j), 1(o)). In contrast, when the phase frustration α_0 is negative, the scale of two chirality clusters is reversed, as shown in Figs. 1(a), 1(f), 1(k).

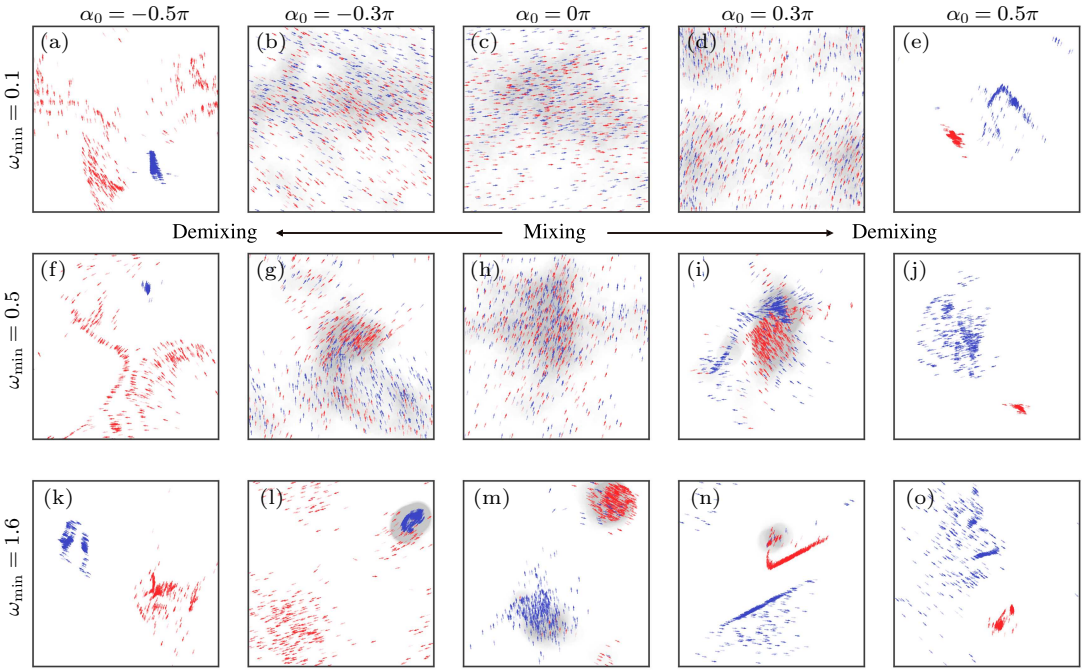


Fig. 1. Snapshots of the spatial distribution for different minimal frequencies $\omega_{\min}$ and phase frustrations α_0. Two types of chiral particles are represented by red ($\omega_i > 0$) and blue ($\omega_i < 0$) arrows, respectively. The position and direction of the arrows represent the spatial position and phase of the particles, respectively. The particles with neighbors of opposite chirality are marked with a gray background.

To further investigate the chiral demixing of the system, we introduced the instantaneous rotational centers $\boldsymbol{c}_i(t) = (X_i(t), Y_i(t))$, which are given by

$$X_i(t) = x_i(t) - \frac{v}{\dot{\theta}_i(t)} \sin\theta_i(t),$$
$$Y_i(t) = y_i(t) + \frac{v}{\dot{\theta}_i(t)} \cos\theta_i(t). \tag{10}$$

By starting from uniform initial conditions, the instantaneous rotational centers of the particles are shown in Figs. 2(a) and 2(b) for the minimal frequency $\omega_{\min} = 1.1$ and phase frustrations $\alpha_0 = 0, -0.5\pi$, respectively. When $\alpha_0 = 0$, the two chiralities are mixed together, and the centers are distributed uniformly in the space, as demonstrated in Fig. 2(a). When $\alpha_0 = -0.5\pi$, it is clearly shown that particles with the same chirality converge into one cluster with increasing time, while particles with opposite chirality exhibit a clear separating effect, i.e., centers with dual chiralities labeled in red and blue approach different ranges, and the scale of the positive and negative chirality clusters is relatively dispersed and compact, as illustrated in Fig. 2(b), which is consistent with the snapshots in Figs. 1(a) and 1(f).

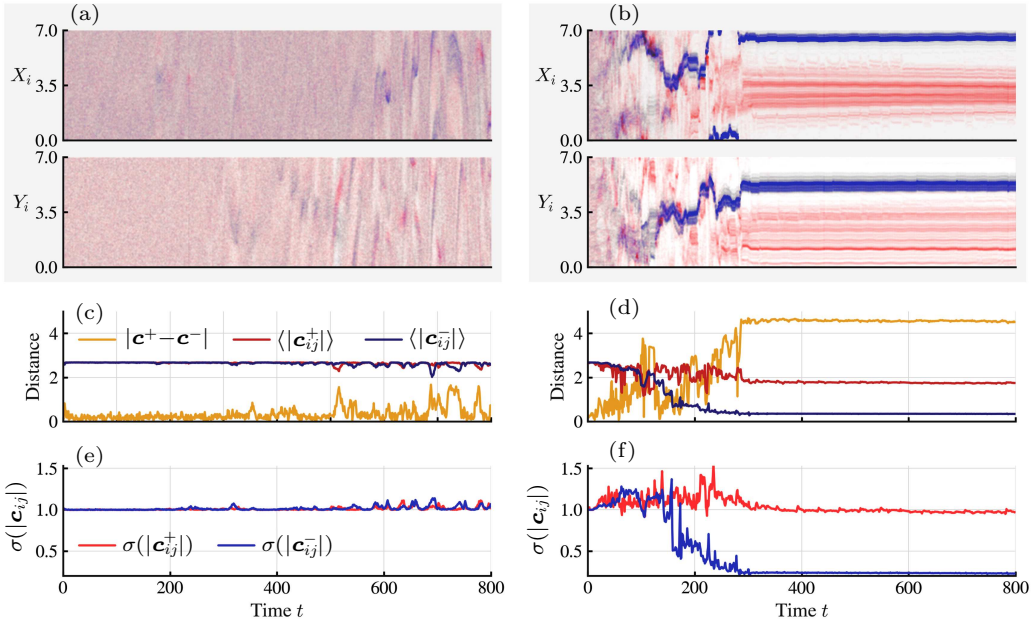


Fig. 2. Demixing behaviors of the system with different phase frustrations α_0 and $\omega_{\min} = 1.1$: (a), (c), (e) $\alpha_0 = 0$; (b), (d), (f) $\alpha_0 = -0.5\pi$. (a), (b) Scatter plot of the instantaneous rotational centers of particles. The color of the dots denotes the corresponding natural frequency. (c), (d) The time evolution of the distance between like/opposite chirality centers. (e), (f) The time evolution of the standard deviation of the distance between like chirality centers.

Some further quantitative analysis is conducted to describe the demixing process of the system. Firstly, the most intuitive metric is the distance between mean centers of two chiralities

$$\left|\boldsymbol{c}^{+}-\boldsymbol{c}^{-}\right|=\left|\frac{1}{N_c}\sum_{i=1}^{N_c}\boldsymbol{c}_i^{+}-\frac{1}{N_c}\sum_{i=1}^{N_c}\boldsymbol{c}_i^{-}\right|, \tag{11}$$

where the notation $\pm$ denotes the positive and negative chiralities, respectively, and $N_c=N/2$ is the number of particles with the same chirality. From the opposite perspective, the mean distance between the centers of the same chirality can describe the compactness of the clusters

$$\langle|\boldsymbol{c}|_{ij}^{\pm}\rangle=\frac{2}{N_c^2}\sum_{i=1}^{N_c}\sum_{j=1}^{i}\left|\boldsymbol{c}_i^{\pm}-\boldsymbol{c}_i^{\pm}\right|. \tag{12}$$

As illustrated in Figs. 2(c) and 2(d), when $\alpha_0=0$, the distance between centers of both like and opposite chirality remains nearly constant. However, for $\alpha_0=-0.5\pi$, there is a notable decrease in the distance between centers of negative chirality, while the distance between centers of different chiralities increases. This observation suggests a phase separation within the system. Furthermore, the standard deviation of the distances between centers of the same chirality,

$$\sigma(|\boldsymbol{c}|_{ij}^{\pm})=\sqrt{\frac{2}{N_c^2}\sum_{i=1}^{N_c}\sum_{j=1}^{i}\left(\left|\boldsymbol{c}_i^{\pm}-\boldsymbol{c}_i^{\pm}\right|-\left\langle|\boldsymbol{c}|_{ij}^{\pm}\right\rangle\right)^2}, \tag{13}$$

can serve as a measure of cluster compactness, as depicted in Figs. 2(e) and 2(f). At $\alpha_0=-0.5\pi$, the standard deviation of the distances between centers within negative chirality is significantly lower, indicating that these clusters are more compact.

In addition to characterizing the time-varying spatial distribution of particles, frustration-varying behaviors can further quantify the ability of the system to demix chiralities, as shown in Fig. 3 with $\omega_{\min}=10^{-3}$. As evident in Fig. 3(a), with the increase of frustration strength $|\alpha_0|$, firstly the distance between the centers of different chiralities is initially close to zero in the mixed state, then bifurcates from zero and increases rapidly at $|\alpha_0|\approx 0.4\pi$, indicating the demixing of the system. Around $|\alpha_0|\approx 0.5\pi$, the distance reaches the maximum, and then decreases slightly with further the increase of $|\alpha_0|$ until it reaches π, where the demixing degree increases again for the phase coupling turning to the exact opposite direction. The distances between the centers of the same chirality also exhibit an opposite trend with the increase of $|\alpha_0|$, as the red and blue lines in Fig. 3(a) show. Moreover, the sign of α_0 exerts different degrees of influence between the two chiralities, where the distance between the centers of the positive chirality is more sensitive to the frustration than that of the negative chirality, when $\alpha_0>0$, and vice versa, which is consistent with the snapshots in Fig. 1 and the results in Fig. 2. This is further confirmed by the standard deviation of distances, as shown in Fig. 3(b). For $\alpha_0>0$, the standard deviation of the distances between centers of the positive chirality decreases with the increase of $|\alpha_0|$, and reaches a minimum close to zero at $\alpha_0\approx 0.5\pi$, which is clearly lower than that of the negative chirality. And this trend is opposite for $\alpha_0<0$.

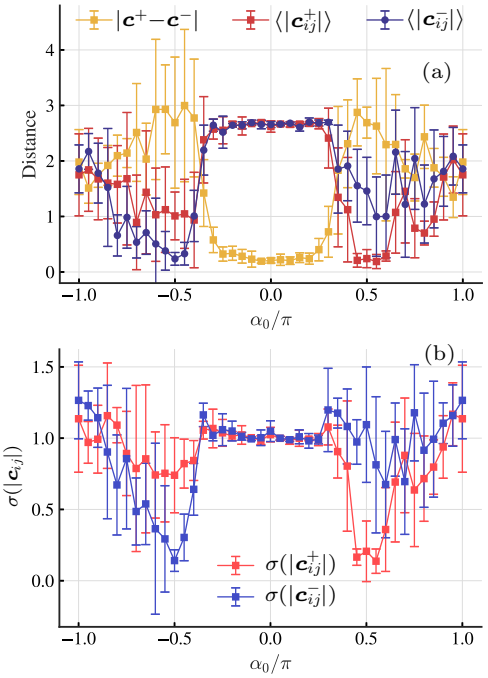


Fig. 3. (a) The distance between centers of neighboring particles versus phase frustration α_0. (b) The standard deviation of distance between centers of neighboring particles versus α_0. All data points are averaged over different initial conditions for $\omega_{\min}=10^{-3}$. Error-bars represent the standard deviations of different initial conditions.

To assess the degree of chiral demixing, we computed the order parameters S and M. The parameter S measures the fraction of neighboring pairs of particles that share the same chirality, while M quantifies the fraction of particles that interact with neighbors exhibiting different chirality. Given the symmetrical role of $\mathrm{sgn}\alpha_0$ in influencing demixing, we focus our presentation on results for α_0 in the range $[-\pi,0]$. Figures 4(a) and 4(b) illustrate the time evolution of the order parameters S and M for various phase frustrations α_0. Here, "$\langle\cdot\rangle$" represents the average computed over the minimum frequency $\omega_{\min}\in[10^{-3},0.5]$. When $\alpha_0=0$, the system remains in a mixed state, with the order parameter S showing a slight decrease and M exhibiting a slight increase over time. For $\alpha_0=-0.4\pi$, the system experiences a phase transition from the mixed state to a demixing state, resulting in a notable increase in S and a corresponding decrease in M. In the case of the most effective frustration, $\alpha_0=-0.5\pi$, both order parameters S and M fluctuate rapidly, quickly reaching a steady state. This behavior indicates that the system has transitioned to a fully phase-separated state, where S attains its maximum value and M reaches its minimum.

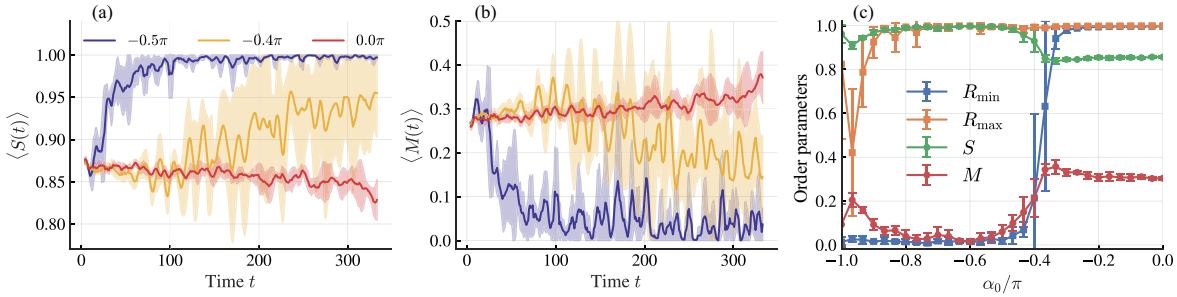


Fig. 4. (a), (b) Time evolution of the order parameters S and M for different phase frustrations α_0, where $\langle\cdot\rangle$ denotes the average taken over the minimal frequency $\omega_{\min} \in [10^{-3}, 0.5]$. (c) Order parameters S, M, $R_{\max}$ and $R_{\min}$ versus α_0 averaged over different initial conditions for $\omega_{\min} = 10^{-3}$. Translucent bond and error-bars represent the standard deviation of values with different minimal frequencies and initial conditions, respectively.

Homoplastically, the order parameters S, M, $R_{\max}$, and $R_{\min}$ as functions of α_0 are presented in Fig. 4(c). The trends in the order parameters S and M align with the time evolution results: S increases while M decreases as $|\alpha_0|$ increases, reaching their respective maximum and minimum values. Following this point, S and M show slight decreases and increases, respectively, indicating a weakening of the demixing effect. Similarly, their trends reverse again as α_0 approaches $-\pi$, where the phase coupling becomes opposite.

Additionally, the order parameters $R_{\max}$ and $R_{\min}$ provide supplementary confirmation of the trends observed in S and M. For weak frustration, both $R_{\max}$ and $R_{\min}$ approach 1, meaning the two chiralities are synchronized, but as frustration intensifies, they diverge to different values. This bifurcation suggests the transition from full phase locking to partial locking within the system. Consistent with the trends of S and M, the difference between $R_{\max}$ and $R_{\min}$ decreases with increasing $|\alpha_0|$ after the maximum point, then increases again until the final reversal at $-\pi$.

4. Phase diagrams and theoretical approximation

To construct the phase diagram of the system, we calculate the order parameters S, M across the phase diagram of $(\alpha_0, \omega_{\min})$ and drive the critical frustrations for the enhancement of chiral demixing, as shown in Fig. 5. The order parameters S and M are color-coded to represent the amplitudes of the order parameters. The dashed lines labeled I and II represent the critical frustrations α_c and α_s, respectively. Line I (α_s) is the critical frustration for the enhancement of clustering, and line II (α_c) is for the chiral demixing. It can be seen that the two critical lines can be well manifested in the phase diagram, where the order parameters S and M exhibit a significant change across the critical lines.

The phase diagram shows that the system is in a mixed state when $\omega_{\min} \ll 1$ and $|\alpha_0| \ll 1$, where the order parameters S and M are close to 0.7 and 1, respectively, corresponding to the region A in Fig. 5. When the minimal frequency $\omega_{\min}$ surmounts the critical line $\alpha_s^{-1}(\omega_{\min})$ (white dashed line), the system will phase separate into two clusters of different chiralities, and the order parameters S increase obviously, while the order parameters M decrease but remain close to 1, which can be seen by comparing the regions B in Figs. 5(a) and 5(b), because the phase separation strengthens the demixing degree, but the coupling between the two chiralities is still strong. When the phase frustration α_0 exceeds the critical line $\alpha_c(\omega_{\min})$ (black dashed line), the system will achieve the complete demixing state, where the order parameters S and M reach their maximum and minimum values, respectively, as shown in the region C in Fig. 5. As the frustration continues to increase, the order parameters S and M decrease and increase slightly, respectively, as the degree of demixing weakens.

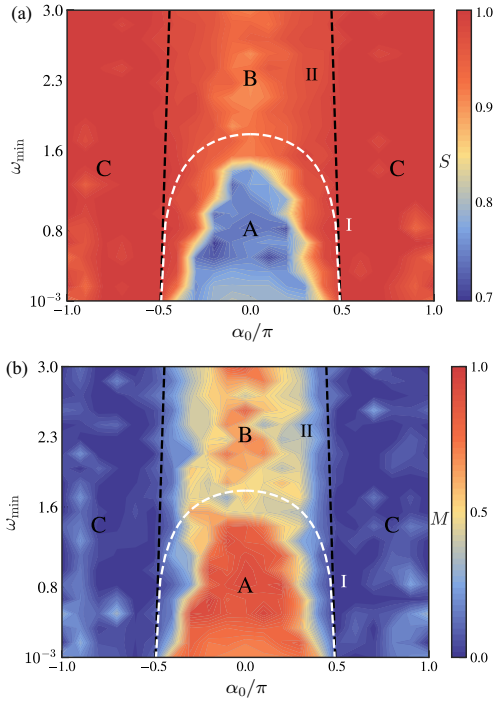


Fig. 5. Heatmaps for order parameters (a) S and (b) M across the phase diagram of $(\alpha_0, \omega_{\min})$ with the critical demixing frustration α_c (black dashed line) and the critical clustering frustration α_s (white dashed line). Different colors describe the amplitudes of the order parameters. The results are averaged over simulations with different initial conditions.

Next we will provide a theoretical approximation to explain the critical frustration for the enhancement of chiral

demixing. The dynamics of the system (1) in the mixing state can be abstracted as a synchronization problem in double-layer phase oscillator networks for its spatially uniform distribution. Therefore, for the translational and rotational invariance of the spatial distribution and the mean-field coupling of the phase, each local subset of connected particles can be regarded equivalently as a group of fully connected oscillators in mean-field coupling. This problem can be described by the following equations:

$$\begin{aligned}\dot{\theta}_i^{\pm} &= \omega_i^{\pm} + \frac{K}{N}\sum_{j=1}^{N_c}\sin\left(\theta_j^{\pm} - \theta_i^{\pm}\right) \\ &+ \frac{K}{N}\sum_{j=1}^{N_c}\left[\sin\left(\theta_j^{\mp} - \theta_i^{\pm} + \alpha_0\right) - \sin\alpha_0\right]. \end{aligned} \tag{14}$$

Each layer $\pm$ represents the particles with the same chirality, and the second and third terms in Eq. (14) describe the intralayer and interlayer interactions, respectively.

In the scenario of the mixing state, the system is in a phase-locked state, where the phase difference between the two layers is fixed. Without loss of generality, let $\theta_i^{\pm}(t) = \theta^{\pm}(t)$ and introduce $\Delta\theta = \theta^{+} - \theta^{-}$, $\Delta\omega = \mu^{+} - \mu^{-}$, the phase locking dynamics of two layers can be reduced to the following equations:

$$\Delta\dot{\theta} = \Delta\omega - 2K\cos\alpha_0\sin\Delta\theta. \tag{15}$$

When $|\Delta\omega| \leqslant 2K|\cos\alpha_0|$, Eq. (15) has fixed-points solutions

$$\Delta\theta = \arcsin\frac{\Delta\omega}{2K\cos\alpha_0}, \tag{16}$$

which means the two layers are phase-locked and the effective frequencies of the two layers are both zero for symmetric natural frequencies. When $|\Delta\omega| > 2K|\cos\alpha_0|$, the two layers are not phase-locked, and the phase difference $\Delta\theta$ will drift with time, which means the raw system is in a demixing state. Therefore, the critical frustration α_c for demixing can be derived as a function of $|\Delta\omega|$ and K

$$\alpha_c = \pm\arccos\frac{|\Delta\omega|}{2K}. \tag{17}$$

The numerical results in Fig. 6 show that the order parameters $R_{\max}$ and $R_{\min}$ exhibit a bifurcation to different values at the critical frustration α_c, and the effective frequencies of the two layers are close to zero when α_0 is less than α_c, and then split into two different values when α_0 exceeds α_c, which agrees well with the theoretical approximation. Furthermore, the theoretical results obtained from the simplified model Eq. (14) can well explain the critical frustration for the raw system in Eq. (1), which is shown as the black dashed line in Fig. 5.

Our previous work gives another insight about the critical frustration α_s for the clustering transition,[57] which is the critical frustration for the clustering of the two chiralities:

$$\alpha_s = \pm\arccos\frac{2\pi d_0\mu^{+}}{K\left(\beta d_0 - r_d\sin\frac{\beta}{2}\right)}, \tag{18}$$

with the terms being

$$\begin{aligned} r_d &= \frac{L}{\sqrt{2}} - d_0 - 2r_o, \\ \beta &= 2\arccos\frac{r_d}{2d_0}, \\ r_o &= \frac{v}{\mu^{+}} = -\frac{v}{\mu^{-}}, \end{aligned} \tag{19}$$

where $\mu^{\pm}$ is the mean natural frequency of the two chiralities. Namely, the critical frustration α_s is the critical frustration for the two swarming clusters to lock phase and merge into one cluster, like the transition from snapshot (m) to (h) in Fig. 1. This solution only holds for the case of $r_d > 0$, which means the two clusters are overlapping. The white dashed line in Fig. 5 represents the critical frustration α_s for the clustering transition, matching well with the transition of order parameters S.

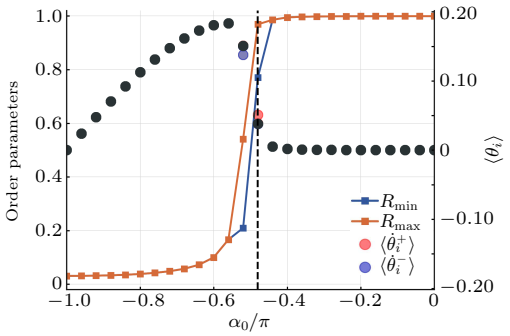


Fig. 6. Order parameters $R_{\max}$, $R_{\min}$ and the effective frequencies of $\pm$ layers versus α_0 for the system in Eq. (14) with $\omega_{\min} = 10^{-3}$. The dark gray dots indicate the effective frequencies where both layers have the same value and the dashed line represents the critical frustration α_c.

Table 1. Numerical critical frustration α_c^* for different system sizes L and N. The last row shows the analytical result from Eq. (16). The values of α_c^* are averaged over different initial conditions, and the standard deviation is shown in the third column.

Variables	$\langle\alpha_c/\pi\rangle$	$\sigma(\alpha_c/\pi)$
$L=4,\ N=1000$	–0.483	0.040
$L=5,\ N=1000$	–0.457	0.033
$L=6,\ N=1000$	–0.493	0.021
$L=7,\ N=1000$	–0.497	0.042
$L=8,\ N=1000$	–0.450	0.062
$L=9,\ N=1000$	–0.497	0.021
$L=7,\ N=2000$	–0.480	0.050
$L=7,\ N=3000$	–0.493	0.013
Analytical	–0.499	–

To assess the validity of the theoretical approximation and quantify finite-size effects, we conducted numerical simulations with $\omega_{\min} = 10^{-3}$, varying the system size through two parameters: the population size N and the spatial box size L. The numerical critical parameter α_c^* is determined as the frustration value at which the difference between $R_{\max}$ and $R_{\min}$

first exceeds 0.97, obtained by gradually decreasing α_0 from 0 to $-\pi$. Since α_s does not exist when $\omega_{min} \ll 1$, we only focus on α_c here. As demonstrated in Table 1, α_c^* exhibits no systematic dependence on N or L, confirming that our results and the corresponding theoretical predictions remain robust in the thermodynamic limit ($N \to \infty$).

5. Conclusions

In this work, we have investigated how inter-chiral frustration influences the demixing dynamics of double-chiral particle mixture, uncovering its pivotal role in enhancing both the transient and steady-state phase separation of chiral active matter. By integrating numerical simulations with theoretical modeling, we demonstrated that introducing frustration between particles of opposite chiralities accelerates the demixing process and amplifies the degree of phase separation. This phenomenon mirrors phase separation in binary mixtures, where frustration-mediated interactions govern the emergence of distinct patterns. Moreover, the sign of frustration plays a crucial role in shaping the spatial scale and compactness of chiral clusters, as evidenced by the quantitative indicators of the distance between rotational centers $\langle|c_{ij}^{\pm}|\rangle$ and the standard deviation of these distances $\sigma(|c_{ij}^{\pm}|)$.

Key findings include the identification of critical frustration thresholds (α_c, α_s) that trigger a sharp transition from mixed to demixed states and the emergence of distinct chiral clusters, as quantified by order parameters S and M. The bifurcation in synchronization metrics (R_{max}, R_{min}) further corroborates the decoupling of chiral clusters at these critical points. Our theoretical framework, grounded in a reduced double-layer oscillator model, successfully predicts these transitions, aligning closely with numerical results and showing insensitivity to finite-size effects.

These insights deepen our understanding of collective behaviors in chiral active matter, with potential applications in designing chiral materials or interpreting biological systems where chirality dictates self-organization. Future studies could explore asymmetric frustration, heterogeneous frustration, or three-dimensional extensions to unravel richer dynamical regimes. Such efforts would bridge the gap between theoretical models and real-world systems, advancing both fundamental and applied research in active matter.

Acknowledgements

Project supported by the National Natural Science Foundation of China (Grant Nos. 12375031 and 11875135), China National University Student Innovation and Entrepreneurship (Grant No. 202410385040), and Fujian University Alliance of Physics Discipline Training Program of Innovation for Undergraduates Development Program, China.

References

[1] Marchetti M C 2015 *Nature* **525** 37
[2] Uchida N and Golestanian R 2010 *Phys. Rev. Lett.* **104** 178103
[3] Walther A and Müller A H E 2008 *Soft Matter* **4** 663
[4] Walther A and Müller A H E 2013 *Chemical Reviews* **113** 5194
[5] Campbell A I, Ebbens S J, Illien P and Golestanian R 2019 *Nat. Commun.* **10** 3952
[6] Ebbens S J and Gregory D A 2018 *Accounts of Chemical Research* **51** 1931
[7] Appert-Rolland C, Pettré J, Olivier A H, Warren W, Duigou-Majumdar A, Pinsard E and Nicolas A 2020 *Collective Dynamics* **5** 1
[8] Helbing D and Molnár P 1995 *Phys. Rev. E* **51** 4282
[9] Gu F, Guiselin B, Bain N, Zuriguel I and Bartolo D 2025 *Nature* **638** 112
[10] Ballerini M, Cabibbo N, Candelier R, Cavagna A, Cisbani E, Giardina I, Lecomte V, Orlandi A, Parisi G, Procaccini A, Viale M and Zdravkovic V 2008 *Proc. Natl. Acad. Sci. USA* **105** 1232
[11] Becker A D, Masoud H, Newbolt J W, Shelley M and Ristroph L 2015 *Nat. Commun.* **6** 8514
[12] Bialek W, Cavagna A, Giardina I, Mora T, Silvestri E, Viale M and Walczak A M 2012 *Proc. Natl. Acad. Sci. USA* **109** 4786
[13] Qiu H, Wei C, Dou R and Zhou Z 2015 *Science China Information Sciences* **58** 1
[14] Chen J, Lei X, Xiang Y, Duan M, Peng X and Zhang H P 2024 *Phys. Rev. Lett.* **132** 118301
[15] Yang X, Ren C, Cheng K and Zhang H P 2020 *Phys. Rev. E* **101** 022603
[16] Jin Y, Wang G, Yuan D, Wang P, Wang J, Chen H, Liu L and Zan X 2023 *Chin. Phys. B* **32** 088703
[17] Liu C, Fu X, Liu L, Ren X, Chau C K, Li S, Xiang L, Zeng H, Chen G, Tang L H, Lenz P, Cui X, Huang W, Hwa T and Huang J D 2011 *Science* **334** 238
[18] Liu G, Patch A, Bahar F, Yllanes D, Welch R D, Marchetti M C, Thutupalli S and Shaevitz J W 2019 *Phys. Rev. Lett.* **122** 248102
[19] Buttinoni I, Bialké J, Kümmel F, Löwen H, Bechinger C and Speck T 2013 *Phys. Rev. Lett.* **110** 238301
[20] Ishimoto K and Gaffney E A 2018 *Scientific Reports* **8** 15600
[21] Navarro R M and Fielding S M 2015 *Soft Matter* **11** 7525
[22] Wang J, Xu T, He J, Chen K and Tian W 2023 *Chin. Phys. B* **32** 070501
[23] Kumar N, Zhang R, de Pablo J J and Gardel M L 2018 *Science Advances* **4** eaat7779
[24] Praetorius S, Voigt A, Wittkowski R and Löwen H 2018 *Phys. Rev. E* **97** 052615
[25] Wächtler C W, Kogler F and Klapp S H L 2016 *Phys. Rev. E* **94** 052603
[26] Kogler F and Klapp S H L 2015 *Europhys. Lett.* **110** 10004
[27] Vissers T, Wysocki A, Rex M, Löwen H, Royall C P, Imhof A and van Blaaderen A 2011 *Soft Matter* **7** 2352
[28] Kudrolli A, Lumay G, Volfson D and Tsimring L S 2008 *Phys. Rev. Lett.* **100** 058001
[29] Riedel I H, Kruse K and Howard J 2005 *Science* **309** 300
[30] Dombrowski C, Cisneros L, Chatkaew S, Goldstein R E and Kessler J O 2004 *Phys. Rev. Lett.* **93** 098103
[31] Yuan D, Wang P, Wang P, Ma X, Wang C, Wang J, Chen H, Wang G and Ye F 2024 *Chin. Phys. B* **33** 060702
[32] Kokot G, Das S, Winkler R G, Gompper G, Aranson I S and Snezhko A 2017 *Proc. Natl. Acad. Sci. USA* **114** 12870
[33] Reinken H, Klapp S H L, Bär M and Heidenreich S 2018 *Phys. Rev. E* **97** 022613
[34] Reichhardt C, Thibault J, Papanikolaou S and Reichhardt C J O 2018 *Phys. Rev. E* **98** 022603
[35] Saintillan D 2018 *Annual Review of Fluid Mechanics* **50** 563
[36] Vicsek T, Czirók A, Ben-Jacob E, Cohen I and Shochet O 1995 *Phys. Rev. Lett.* **75** 1226
[37] Liebchen B and Levis D 2017 *Phys. Rev. Lett.* **119** 058002
[38] Brokaw C J, Luck D J and Huang B 1982 *Journal of Cell Biology* **92** 722
[39] Kamiya R and Witman G B 1984 *Journal of Cell Biology* **98** 97
[40] Mano T, Delfau J B, Iwasawa J and Sano M 2017 *Proc. Natl. Acad. Sci. USA* **114** E2580
[41] Kümmel F, ten Hagen B, Wittkowski R, Buttinoni I, Eichhorn R, Volpe G, Löwen H and Bechinger C 2013 *Phys. Rev. Lett.* **110** 198302

[42] Kümmel F, ten Hagen B, Wittkowski R, Takagi D, Buttinoni I, Eichhorn R, Volpe G, Löwen H and Bechinger C 2014 *Phys. Rev. Lett.* **113** 029802

[43] Mokashi-Punekar S, Zhou Y, Brooks S C and Rosi N L 2020 *Advanced Materials* **32** 1905975

[44] Mokashi-Punekar S, Zhou Y, Brooks S C and Rosi N L 2020 *Advanced Materials* **32** 1905975

[45] Jennings H S 1901 *The American Naturalist* **35** 369

[46] Jiang M, Zhou A, Chen R, Yang Y, Dong H and Wang W 2023 *Phys. Rev. E* **107** 024411

[47] Tan T H, Mietke A, Li J, Chen Y, Higinbotham H, Foster P J, Gokhale S, Dunkel J and Fakhri N 2022 *Nature* **607** 287

[48] Mauleon-Amieva A, Allen M P, Liverpool T B and Royall C P 2023 *Science Advances* **9** eadf5144

[49] Han M, Yan J, Granick S and Luijten E 2017 *Proc. Natl. Acad. Sci. USA* **114** 7513

[50] Zhang B, Sokolov A and Snezhko A 2020 *Nat. Commun.* **11** 4401

[51] Li Y, Li L, Marchesoni F, Debnath D and Ghosh P K 2020 *Phys. Rev. Res.* **2** 013250

[52] Liebchen B, Cates M E and Marenduzzo D 2016 *Soft Matter* **12** 7259

[53] Levis D, Pagonabarraga I and Liebchen B 2019 *Phys. Rev. Res.* **1** 023026

[54] Ventejou B, Chaté H, Montagne R and Shi X Q 2021 *Phys. Rev. Lett.* **127** 238001

[55] Wang Y, Ventéjou B, Chaté H and Shi X Q 2024 *Phys. Rev. Lett.* **133** 258302

[56] Fruchart M, Hanai R, Littlewood P B and Vitelli V 2021 *Nature* **592** 363

[57] Lu Y, Xu Y, Cai W, Tian Z, Xu J, Wang S, Zhu T, Liu Y, Wang M, Zhou Y, Yan C, Li C and Zheng Z 2025 *Chaos, Solitons & Fractals* **191** 115794

[58] Li J J, Guo R X and Ai B Q 2024 *Phys. Rev. E* **110** 024608

[59] Ai B Q, Quan S and Guo Li F 2023 *New J. Phys.* **25** 063025

[60] Li J R, Zhu W j, Li J J, Wu J C and Ai B Q 2023 *New J. Phys.* **25** 043031

[61] Scholz C, Engel M and Pöschel T 2018 *Nat. Commun.* **9** 931

[62] Nguyen N H P, Klotsa D, Engel M and Glotzer S C 2014 *Phys. Rev. Lett.* **112** 075701

[63] Darnton N, Turner L, Breuer K and Berg H C 2004 *Biophysical Journal* **86** 1863

[64] Kim M J and Breuer K S 2006 *Journal of Fluids Engineering* **129** 319

[65] Dreyfus R, Baudry J, Roper M L, Fermigier M, Stone H A and Bibette J 2005 *Nature* **437** 862

[66] Tierno P, Golestanian R, Pagonabarraga I and Sagués F 2008 *Phys. Rev. Lett.* **101** 218304

[67] Palaia I and Šarić A 2022 *The Journal of Chemical Physics* **156** 194902

[68] Levis D and Liebchen B 2019 *Phys. Rev. E* **100** 012406

[69] Chakraborty S, Das M K, Bubnov A, Węgłowska D and Dabrowski R 2019 *J. Mater. Chem. C* **7** 10530

[70] Kim D, Kim W, Park E, Mattern N and Eckert J 2013 *Progress in Materials Science* **58** 1103